Isolating mesoscale coupled ocean–atmosphere interactions in the Kuroshio Extension region

Dian A. Putrasahan [a,*], Arthur J. Miller [a], Hyodae Seo [b]

[a] *Scripps Institution of Oceanography, University of California, San Diego, La Jolla, CA 92093-0224, USA*
[b] *Woods Hole Oceanographic Institution, Woods Hole, MA 02543, USA*

A B S T R A C T

The Kuroshio Extension region is characterized by energetic oceanic mesoscale and frontal variability that alters the air–sea fluxes that can influence large-scale climate variability in the North Pacific. We investigate this mesoscale air-sea coupling using a regional eddy-resolving coupled ocean–atmosphere (OA) model that downscales the observed large-scale climate variability from 2001 to 2007. The model simulates many aspects of the observed seasonal cycle of OA coupling strength for both momentum and turbulent heat fluxes. We introduce a new modeling approach to study the scale-dependence of two well-known mechanisms for the surface wind response to mesoscale sea surface temperatures (SSTs), namely, the 'vertical mixing mechanism' (VMM) and the 'pressure adjustment mechanism' (PAM). We compare the fully coupled model to the same model with an online, 2-D spatial smoother applied to remove the mesoscale SST field felt by the atmosphere. Both VMM and PAM are found to be active during the strong wintertime peak seen in the coupling strength in both the model and observations. For VMM, large-scale SST gradients surprisingly generate coupling between downwind SST gradient and wind stress divergence that is often stronger than the coupling on the mesoscale, indicating their joint importance in OA interaction in this region. In contrast, VMM coupling between crosswind SST gradient and wind stress curl occurs only on the mesoscale, and not over large-scale SST gradients, indicating the essential role of the ocean mesocale. For PAM, the model results indicate that coupling between the Laplacian of

* Corresponding author. Present address: Rosenstiel School of Marine and Atmospheric Sciences, University of Miami, Miami, FL 33149-1098, USA. Tel.: +1 305 421 4074.
E-mail addresses: dputrasahan@rsmas.miami.edu, dputrasa@ucsd.edu (D.A. Putrasahan).

sea level pressure and surface wind convergence occurs for both mesoscale and large-scale processes, but inclusion of the mesoscale roughly doubles the coupling strength. Coupling between latent heat flux and SST is found to be significant throughout the entire seasonal cycle in both fully coupled mode and large-scale coupled mode, with peak coupling during winter months. The atmospheric response to the oceanic mesoscale SST is also studied by comparing the fully coupled run to an uncoupled atmospheric model forced with smoothed SST prescribed from the coupled run. Precipitation anomalies are found to be forced by surface wind convergence patterns that are driven by mesoscale SST gradients, indicating the importance of the ocean forcing the atmosphere at this scale.

1. Introduction

In the western North Pacific Ocean, where major ocean currents meet along the eastern coast of Japan, meandering sea surface temperature (SST) fronts form. From the south, a strong and warm western boundary current hugs the Southeastern coast of Japan and separates around $35°$ N to form the Kuroshio Extension (KE). Within the KE, pronounced SST fronts produce climatological SST gradients steeper than $3°C/100\,km$ (Tokinaga et al., 2009), with synoptic fronts that are much stronger, that consequently impact the surface flux exchanges with the atmosphere. The long-term variability of these flux anomalies in the KE region are known to be important in influencing large-scale decadal North Pacific climate feedback processes (Miller and Schneider, 2000; Latif, 2006; Kwon et al., 2010; Frankignoul et al., 2011; Taguchi et al., 2012).

Satellite observation-based studies have shown the strong influence of the mesoscale SST distribution upon the overlying atmospheric wind and wind stress patterns (Xie, 2004; Small et al., 2008; Chelton et al., 2004; Chelton and Xie, 2010). Observations have also indicated coupling between SST and surface heat fluxes (e.g. Thum et al., 2002; Vecchi et al., 2004; Liu et al., 2007; Seo et al., 2008) and models have shown that latent and sensible heat fluxes into the ocean have a negative correlation with mesoscale SSTs in various parts of the World Ocean (e.g. Seo et al., 2007; Haack et al., 2008; Bryan et al., 2010), which suggests SST forcing the atmosphere (Wu et al., 2006) as opposed to the historical atmospheric role in driving large-scale SST anomalies (e.g. Cayan, 1992). It is important to understand the character and mechanisms controlling these regional mesoscale flux anomalies in order to gain further insight into coupling processes controlling large-scale climate variations.

In this study, we execute novel regional ocean–atmosphere coupled modeling experiments that include and exclude the impact of oceanic mesoscale eddies, in order to isolate their effect on the strength of ocean–atmosphere (OA) coupling and local atmospheric response. This is achieved using an interactive 2-D spatial smoother of SST that removes the mesoscale SST structures felt by the atmosphere, while leaving the ocean free to develop mesoscale eddies. The new modeling strategy allows us to quantify the spatial scale over which the coupling processes affect surface fluxes and atmospheric boundary layer fields of winds, vertical velocity, and precipitation. The modeling results are supported by a complementary analysis of observed SST, wind stress, and surface heat flux anomalies that together provide estimates of the seasonal air–sea coupling over the KE region.

The model furthermore allows us to study two prominent mechanisms that have been proposed to explain the response of wind in SST frontal regions, namely the 'vertical mixing mechanism' (VMM) and the 'pressure adjustment mechanism' (PAM). The VMM suggests that warmer (colder) SST reduces (enhances) the stability of the overlying atmosphere, which enhances (inhibits) the downward transfer of momentum through mixing, that would thus increase (decrease) surface wind stress (Wallace et al., 1989) over the SST anomalies. When winds blow parallel or perpendicular to an SST front, it can lead to wind stress divergence along the downwind, or curl along the crosswind, SST gradients (Chelton

et al., 2001, 2004). In contrast, the PAM suggests that warm (cold) SST anomalies induce low (high) surface pressure anomalies that would promote convergence (divergence) of surface winds over the SST anomalies (Lindzen and Nigam, 1987). The relative importance of these two processes (Takatama et al., 2011) may potentially alter the way the atmosphere responds to oceanic variability in the KE region.

In the next section, we explain the satellite observations. In Section 3, the modeling strategy is introduced and the experiments delineated. Section 4 describes the results, and a summary is given in Section 5.

2. Satellite observations

Satellite observations are used to identify OA coupling in the KE region and verify the model output. For the satellite data, SST measurements are obtained from fusion of data from the Tropical Rainfall Measuring Mission (TRMM) Microwave Imager (TMI), which was launched in November 1997 (Wentz et al., 2000), and from the Advanced Microwave Scanning Radiometer on the Earth Observing System (EOS) Aqua satellite (AMSR-E), that was launched in May 2002 (Chelton and Wentz, 2005). We use the daily, 0.25° resolution, combined TMI and AMSRE data that are available from Remote Sensing Systems (RSS). Wind stress products are derived from the Quick Scatterometer (QuikSCAT) satellite (Freilich et al., 1994), which was in operation from July 1999 till November 2009. We use daily, 0.5° resolution wind stress products, which are also available through RSS. The Woods Hole Oceanographic Institution (WHOI) Objectively Analyzed Air–Sea Heat Fluxes (OAflux) project provides surface latent and sensible heat fluxes constructed from observed satellite fields and three atmospheric reanalyzes, at 1° resolution from 1985 onwards (Yu and Weller, 2007).

3. Coupled model experiments

The Scripps Coupled Ocean–Atmosphere Regional (SCOAR) model is employed to perform the coupled air–sea interaction studies in the KE region. The model consists of the Experimental Climate Prediction Center (ECPC) Regional Spectral Model (RSM, Juang and Kanamitsu, 1994) as the atmospheric component, the Regional Ocean Modeling System (ROMS, Shchepetkin and McWilliams, 2005; Haidvogel et al., 2008) as the oceanic part, and a flux-SST coupler built by Seo et al. (2007) to bridge the two. Currently, the coupling works in a sequential manner, such that RSM and ROMS run individually and alternatively, exchanging forcing fields at specified increments. For this study, the ocean and atmosphere are coupled on a daily timescale. The SCOAR model is chosen because it has been shown to be effective in capturing mesoscale coupling in tropical and mid-latitudinal oceans (Seo et al., 2006, 2008).

The model domain chosen covers a regional grid of the western North Pacific that includes Japan and the Kuroshio Extension (125–165° E, 31–47° N). The atmospheric and ocean model have the same horizontal grid with 25 km resolution and matching land-sea mask. The atmosphere has 28 vertical layers whilst the ocean has 30 layers. The vertical coordinates for the ocean model were stretched to give higher resolution to the surface layers. The ocean spin up (in uncoupled mode) is forced by National Centers of Environmental Prediction Reanalysis-2 (NCEP R2 (Kanamitsu et al., 2002)) winds from 1980 to 2000 to allow equilibration before any runs are performed. NCEP R2 is used as boundary conditions for the atmosphere, such that the model provides a dynamic downscaling of observations. Oceanic boundary conditions are taken from monthly Japan Agency for Marine-Earth Science and Technology (JAMSTEC) Ocean General Circulation Model for the Earth Simulator (OFES) dataset provided by The Earth Simulator Center, JAMSTEC (Sasaki et al., 2006). We run the coupled model for 8 years (commencing in 2000), giving one year to allow the coupled system to equilibrate, thereby providing a 7-year (2001–2007) daily output of the oceanic and atmospheric state. This model run overlaps the satellite observed time period for 2003–2007.

In order to isolate the impact of mesoscale SST on the coupling, we employ a novel strategy. We execute a 'Smoothed SCOAR' run, in which we interactively smooth the SST that is felt by the atmosphere, over the same time period and same resolution as the fully coupled 'Control SCOAR' run.

Note that the actual SST in the ocean model is left unchanged but evolves instead under the influence of the atmosphere that has seen only the smoothed SST field. In the experiments that remove the mesoscale air–sea interactions, an online 2-D spatial, locally weighted scatterplot smoothing (lowess) filter (Cleveland, 1979; Schlax et al., 2001) is applied to the SST field that forces RSM at each coupling step. This procedure allows large-scale SST coupling to be preserved while extinguishing the mesoscale eddy impacts on the atmospheric boundary layer. This technique allows us to separate the spatial scales of air–sea coupling by comparing with the fully coupled run. Here we choose a 5-degree lowess filter, which yields an effective cutoff wavelength of $3.0°$ ($\sim$300 km) in latitude and longitude. As such, features up to 300 km are considered mesoscale and greater than 300 km are referred to as large scale.

Since the ocean mesoscale eddies in Control SCOAR and Smoothed SCOAR are random and uncorrelated, we also used a deterministic approach to further isolate the effects of these mesoscale SST patterns on the atmosphere. This was achieved by applying the 2-D smoother upon the raw SST fields from the fully coupled SCOAR run (Control SCOAR) and using these daily smoothed SST fields as prescribed surface forcing for the uncoupled atmosphere (Smoothed RSM) to obtain an 8-year (2000–2007) daily response of the atmospheric state. The deterministic difference in the two runs highlights the influence of mesoscale SST on the overlying atmosphere, as well as isolating the mesoscale coupling effects.

4. Results and discussion

The Control SCOAR produces a strong Kuroshio current and vigorous mesoscale eddy field that yields meandering SST fronts (Fig. 1a) similar to those observed in nature. The Smoothed SCOAR run also produces a strong Kuroshio and a similarly energized mesoscale in the ocean (not shown). The smoothed SST seen by the atmosphere in Smoothed SCOAR (Fig. 1b) however, while exhibiting broad-scale SST anomalies, does not include the mesoscale features in SST, as expected by this strategy. For our analysis, we focus on the strongly energetic open-ocean eddy region (34–40° N, 145–163° E, boxed domain in Fig. 1a), which is far from the (physical) western boundary as well as the (specified) open boundaries.

4.1. SST-wind stress coupling through vertical mixing mechanism

The strength of the VMM can be quantified following Chelton et al. (2001) by estimating the linear relationship between wind stress divergence and downwind SST gradients, and represented as the coupling coefficient, s_d. At each grid point in the box, we computed these fields, binned them, and plotted the mean from each bin in a scatter diagram with error bars indicating plus-or-minus one standard deviation. A regression coefficient (hereafter called the coupling coefficient) was then computed from the slope of the linear fit to the mean values of each bin, along with the standard error of the slope, a p-value, and a squared correlation coefficient (r^2). We consider a slope to be significant if the p-value is less than 0.05 and at least 50% of the variance is explained by the linear relation (equivalent to r^2 greater than 0.5), the latter criterion being a measure of the physical usefulness of the relation. Note that no spatial highpass filtering of the observations or the model output was performed in this procedure, unlike previous studies (Chelton et al., 2001, 2004; O'Neill et al., 2003). By retaining both large scale and mesoscale SSTs in VMM, we are able to assess their relative role in coupling strength.

Fig. 2a shows an example of coupling between wind stress divergence and downwind SST gradients for January 2006. Over the active mesoscale eddy region, the Control run, Smoothed run and observations all exhibit significant coupling, with $s_d = 1.12 \pm 0.02$, $s_d = 1.71 \pm 0.09$, $s_d = 1.07 \pm 0.11$, respectively. The rough comparability between model and observation is an indication that SCOAR is quantitatively well representing the observed surface flux coupling processes. Control SCOAR and Smoothed SCOAR each produce coupling coefficients that, surprisingly, are within 50% of each other. The range of SST gradients in Smoothed SCOAR ($\pm 3\,°C/100$ km) is smaller than in the Control SCOAR ($\pm 5\,°C/100$ km), yet even these weaker large-scale temperature gradients can have a significant influence on the regional wind stress divergence. Also, the scatter of points in Control SCOAR is much more than in Smoothed

SCOAR, which is likely attributed to the presence of oceanic mesoscale eddies and its feedback onto the atmosphere.

This analysis was repeated for every month of 2003–2007 and a time series of the coupling coefficients is plotted in Fig. 2b, along with the standard error of each coupling coefficient represented by the error bars. All three cases, Control SCOAR, Smoothed SCOAR and observations, indicate that the coupling has a seasonal cycle with a pronounced and significant peak in the winter season (DJFM) when both the winds strengthen and the vertical stability of the atmosphere is weaker than in summer. During summer months, the coupling is near zero and not significant. In winter months, however, the model exhibits coupling estimates that are higher than observations by roughly a factor of two. Possible reasons for this model-data mismatch are (i) model errors, (ii) noise in the observations, (iii) systematic undersampling in the wind stress observations (50 km resolution) due to smoothing of the mesoscale features that may yield a stronger coupling, or (iv) model-data differences in the random mesoscale SST distribution leading to potential biases in the scale or strength of model SST anomalies and their phasing with the ambient wind field.

To better understand the seasonal cycle of the coupling coefficients, we plot the distribution of wind stress and SST (Fig. 3) for a typical winter (January 2006) and summer month (July 2005), as well as their corresponding wind stress divergence and downwind SST gradients patterns (Fig. 4). Fig. 3 indicates prevailing westerlies in winter and southerlies in summer, with larger wind stresses in winter compared to summer. In Fig. 4, the patterns co-locate similarly for summer and winter months, indicating no preferential difference in response to the alteration of the prevailing wind direction. Also, for a given SST gradient, the magnitude of the wind stress divergence is much weaker in summer than
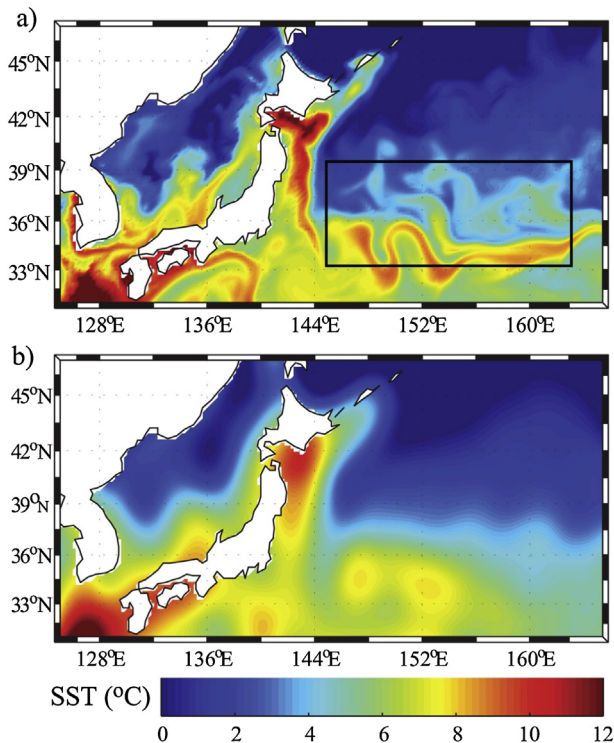

Fig. 1. Averaged SST distribution during January 2006, over entire model domain for Control SCOAR (top) and Smoothed SCOAR (bottom). Boxed region is the active eddy region (KE region [34–40° N, 145–163° E]) for which analysis are performed.
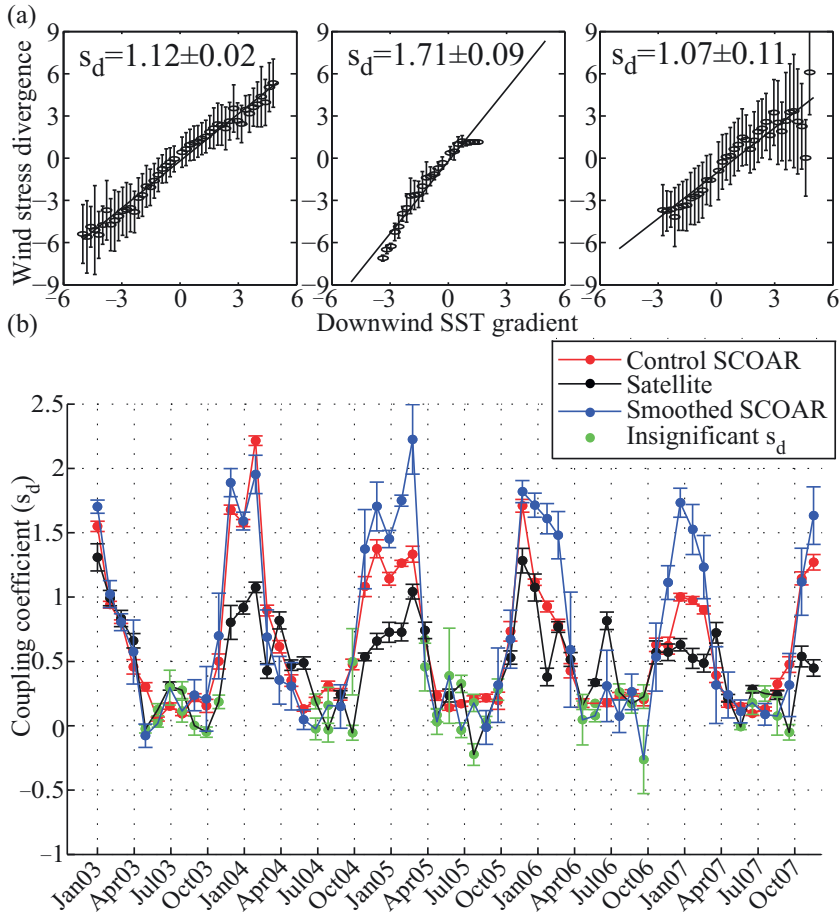
Fig. 2. (a) Linear fit to the bin-scatter plot of wind stress divergence (N/m^2 per 10,000 km) against downwind SST gradients (°C per 100 km) over the KE region (34–40° N, 145–163° E), averaged during January 2006, for Control SCOAR (left), Smoothed SCOAR (middle) and observations (right), along with their coupling coefficients (s_d). Error bars are one standard deviation from the mean of each bin; (b) time series of monthly s_d for 2003–2007, for Control SCOAR (red), Smoothed SCOAR (blue) and observations (black). Error bars represent standard error of the slopes. Green dots indicate s_d with r^2 value smaller than 0.5 and p-value greater than 0.05. (For interpretation of the references to color in this figure legend, the reader is referred to the web version of the article.)

in winter. This suggests that the much weaker vertical stability of the atmosphere in winter, and not the direction of winds, is the main controlling influence on the sensitivity of the atmosphere to SST anomalies in this region. To further validate this interpretation, we compute the monthly low-level thermal stability (not shown), based on the temperature difference between 925 hPa and the surface, over the region and find that the atmospheric stability is indeed weakest in January and strongest in June–July.

The scale-dependence experiments indicate that the coupling coefficient is not entirely attributable to coupling at the oceanic mesoscale. Rather, even large-scale SST gradients can produce a potentially important impact on the regional atmospheric boundary layer (ABL) response. The magnitude of the coupling coefficient in Smoothed SCOAR is larger than in Control SCOAR, which is a surprisingly result. This may be due to the presence of the large-scale Kuroshio SST front generating persistent large-scale SST anomalies that imprint the ABL. On the other hand, the largest divergence anomalies
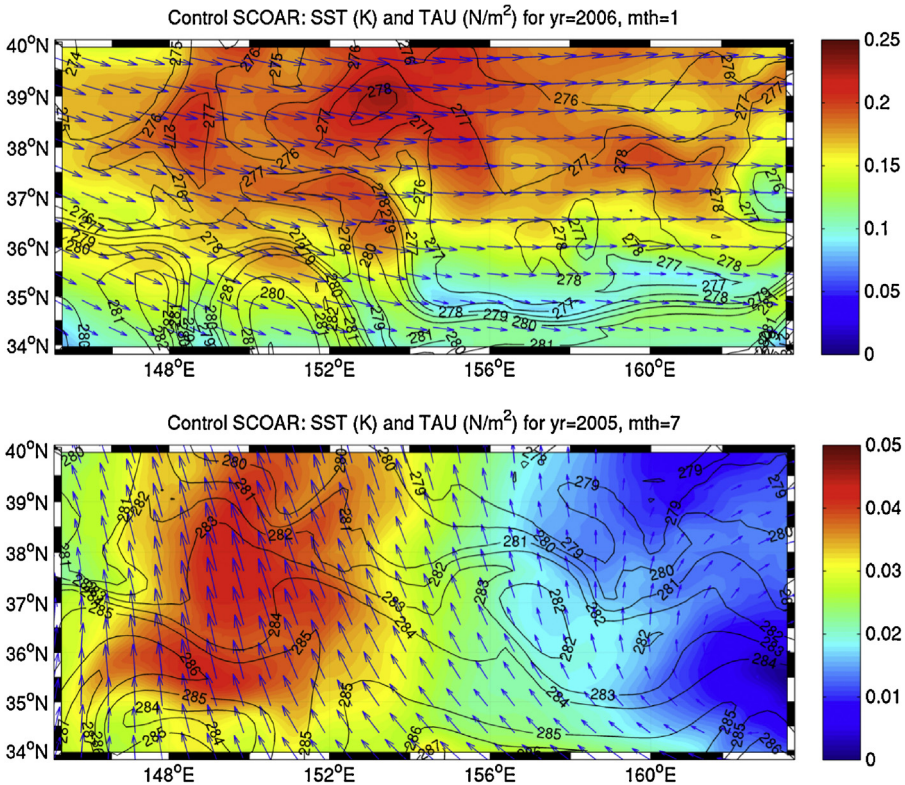
Fig. 3. Colormap and vectors of wind stress (N/m^2) for a winter (January 2006) and summer (July 2005) month, overlaid with contours of SST (K).

occur in Control SCOAR, which is indicative of the strong impact of the local mesoscale SST anomalies in influencing the ABL.

The crosswind SST gradient relationship with wind stress curl (Chelton et al., 2001, 2004) is also investigated following the same procedure. Fig. 5a reveals significant wintertime coupling of these variables for Control SCOAR and observations. Again, the model tends to produce coupling coefficients (s_c) that are similar, or somewhat larger, in amplitude than the observations. However, the coupling coefficients from Smoothed SCOAR are either nearly zero, or indistinguishable from zero based on the error bars, for all seasons (Fig. 5b). The smoothing has revealed the vital importance of mesoscale SST on this relationship. Large-scale model SST gradients are incapable of imprinting their signature on the large-scale wind stress curl field. This may be due to the wind stress curl field of synoptic-scale geostrophic winds obscuring the influence of the large-scale SST. This is in contrast to the result for large-scale SST gradients affecting wind stress divergence. The divergence field associated with intrinsic synoptic-scale variability may be sufficiently small to allow even the large-scale SST imprint to be detected.

4.2. SST-wind coupling through pressure adjustment mechanism

Studies have shown pressure adjustment mechanism (PAM) works in strong SST frontal regions (Minobe et al., 2008, 2010; Takatama et al., 2011; Shimada and Minobe, 2011), for which SST anomalies induce pressure anomalies accompanied with anomalies in wind convergence. Fig. 6 shows difference
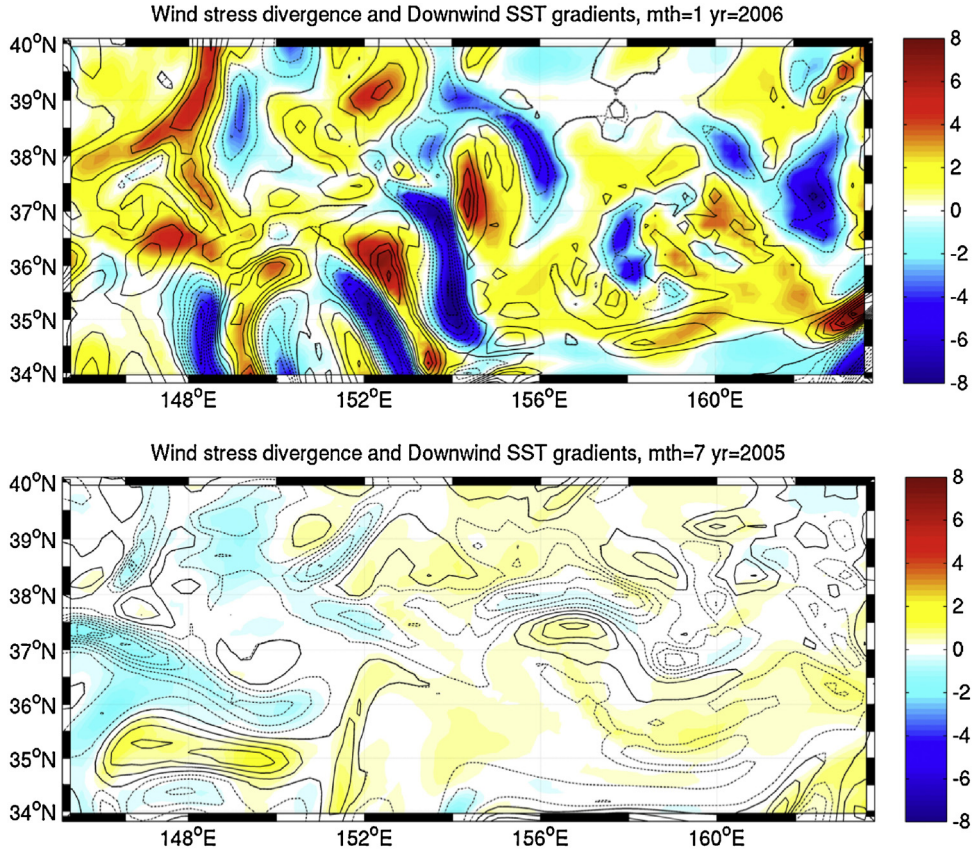
Fig. 4. Colormaps of wind stress divergence (N/m^2 per 10,000 km) overlaid with contours of downwind SST gradients (°C per 100 km) averaged for winter of January 2006 (top panel) and summer of July 2005 (bottom panel) for the KE region. Solid (dashed) contours denote positive (negative) downwind SST gradients, with contour intervals of 1 °C per 100 km.

in SLP overlaid with difference in SST between Control SCOAR and Smoothed SCOAR for the KE region. Top panel is averaged over a typical winter month, January 2006, and the bottom panel is averaged over a typical summer month, July 2005. In winter, SLP perturbations generally follow SST perturbations, with cooler (warmer) SST inducing high (low) pressure anomalies by approximately −7 Pa/°C. In summer, the alignment is less clear, but the general distribution agrees well, in that low (high) pressure changes correspond to positive (negative) SST changes by about −2 Pa/°C. We also tested whether the SLP perturbations follow a linear hydrostatic response to SST anomalies be reconstructing the SLP using the hydrostatic equation with air density variations integrated from surface to 925 hPa height and approximated by Eq. (2b) of Lindzen and Nigam (1987). The reconstructed SLP strongly corresponds to the pattern of the model SLP, with magnitudes slightly overestimated. These results suggest that the pressure adjustment mechanism is active in the simulations.

Typically, the SLP Laplacian, SST Laplacian and wind convergence are used to quantify the pressure adjustment mechanism (Minobe et al., 2008; Shimada and Minobe, 2011). Fig. 7 reflects PAM occurrence in the KE region via the collocation of SLP Laplacian with negative SST Laplacian and wind convergence. It reinforces the notion that warm (cool) SST anomalies concomitantly induce low (high) pressure anomalies and low level wind convergence (divergence). For a more
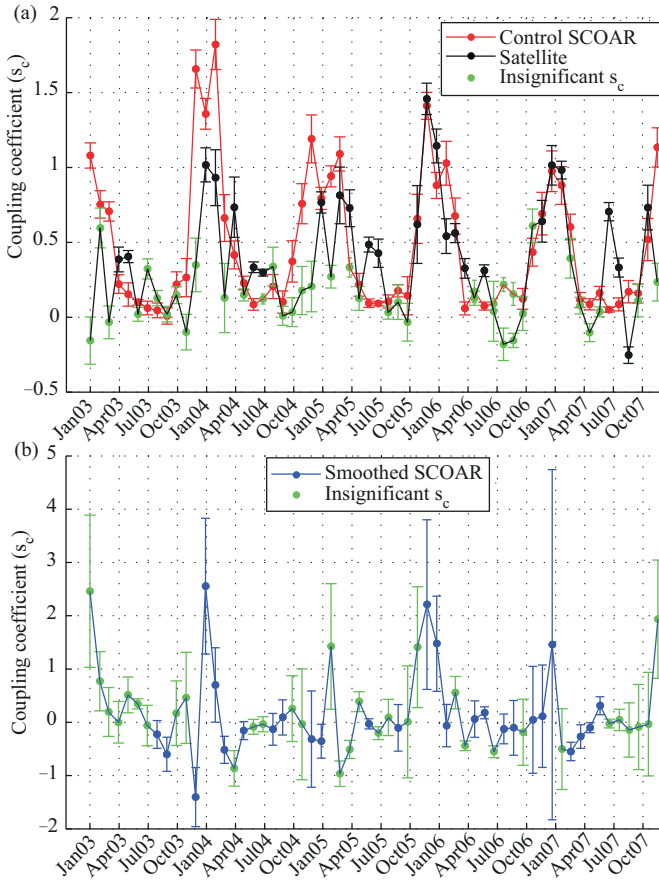
Fig. 5. (a) Time series of monthly coupling coefficients between crosswind SST gradients (°C per 100 km) and wind stress curl (N/m^2 per 10,000 km), s_c, for 2003–2007, for Control SCOAR (red) and observations (black). Error bars represent standard error of the slopes. Green dots indicate s_c with r^2 value smaller than 0.5 and p-value greater than 0.05; (b) same as above except this is for Smoothed SCOAR (blue). Error bars represent standard error of the slopes. Green dots indicate s_c with r^2 value smaller than 0.5 and p-value greater than 0.05. (For interpretation of the references to color in this figure legend, the reader is referred to the web version of the article.)

quantitative approach, we investigate PAM in the KE region by computing the linear relationship of 10 m wind convergence and sea level pressure (SLP) Laplacian over the same active eddy region as the previous SST-wind stress analysis. The strength of the coupling is measured by the slope of the linear fit to the bin-scatter plot of corresponding variables, and we designate the slope as the coupling coefficient, s_p. Both Control SCOAR and Smoothed SCOAR exhibit a significant linear relation of wind convergence to SLP Laplacian (Fig. 8a), with coupling coefficients of $s_p = 2.38 \pm 0.09$ and $s_p = 1.58 \pm 0.07$ respectively for the month of January 2006. A larger coupling coefficient in Control SCOAR suggests that the mesoscale coupling heightens the linear relationship of SLP Laplacian to wind convergence.

For each month of 2003–2007, we computed the coupling coefficient that reflects the PAM and its time evolution. Fig. 8b illustrates the seasonal cycle of this coupling, with peaks during winter seasons. The winter peaks are again likely due to the much weaker vertical stability of the atmosphere in winter, which allows a higher sensitivity to SST anomaly forcing.
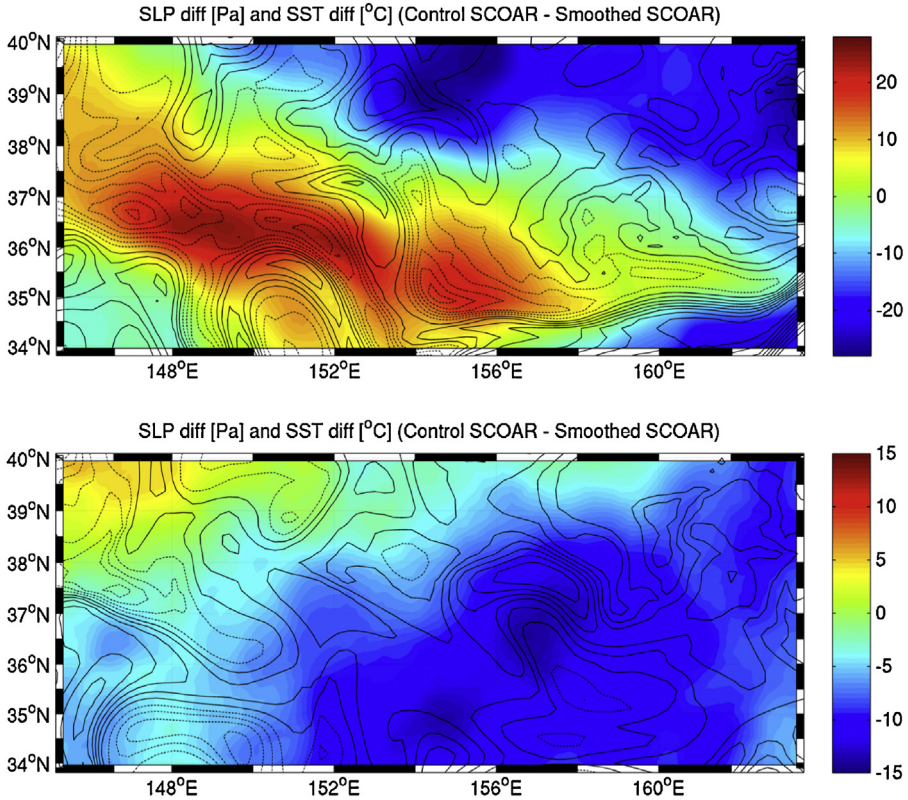
Fig. 6. Top panel: Colormap of SLP (Pa) difference overlaid with contours of SST (°C) difference between Control SCOAR and Smoothed SCOAR, averaged over January 2006. Contour intervals for SST difference are 0.5 °C, with solid (dashed) lines representing positive (negative) values. Bottom panel: Same as top panel, except averaged for July 2005.

Control SCOAR consistently produces higher coupling coefficients than Smoothed SCOAR, suggesting that large-scale coupling through this mechanism is not as significant as mesoscale coupling, in contrast to the VMM divergence, where large-scale coupling plays a significant role.

It should be noted that PAM requires a change in the heat content of the entire ABL induced over the SST front, for which this does not occur in an instantaneous fashion. As such, the spatio-temporal evolution of the ABL over an SST front may be better understood with a Lagrangian approach, which would allow identification of equilibrium time-scale and lagged response of ABL over the SST front. In a simplified case with the cross-equatorial flow over the eastern Pacific, a steady-state quasi-Lagrangian LES modeling by De Szoeke and Bretherton (2004) suggests the dominance of the VMM mechanism via a more rapid adjustment of static stability to air–sea temperature difference and heat flux. It is possible that the PAM mechanism may manifest more strongly in the downstream of the SST because the short residence time of the air mass given the mean wind speed implies an insufficient time for the SST to influence the mass and moisture within the whole ABL to produce substantial SLP anomalies. In KE region where the alignment of wind and SST front varies more dramatically, this type of steady quasi-Lagrangian modeling may be difficult unless existing sophisticated feature tracking algorithms of vorticity and SST are employed. While this merits for further research, it is beyond the scope of this study.
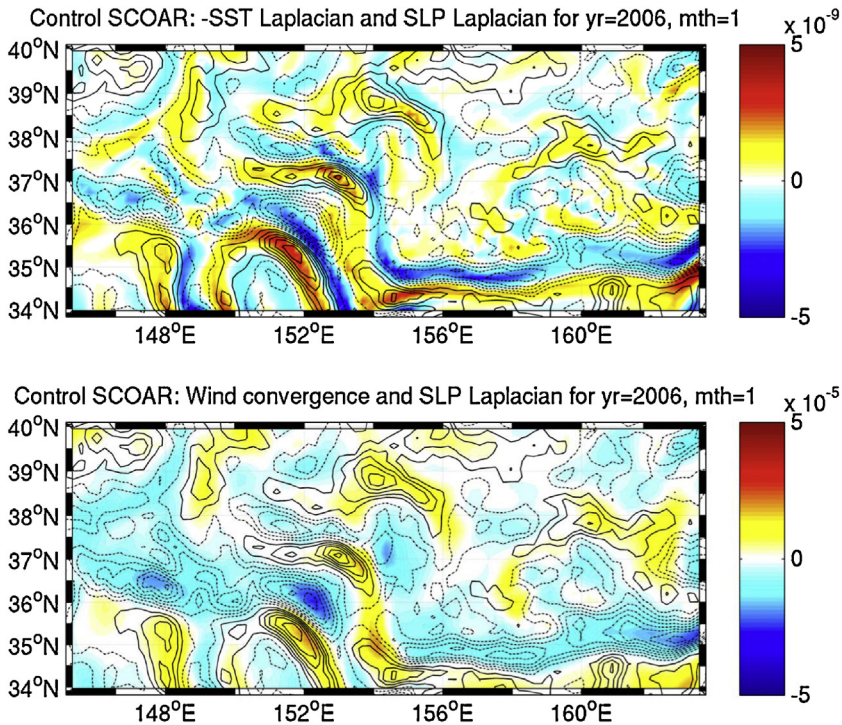
Fig. 7. Top panel: Colormap of negative SST Laplacian ($\circ$C/m^2) overlaid with contours of SLP Laplacian (1×10^{-9} Pa/m^2 intervals), for Control SCOAR over the KE region, averaged over January 2006. Solid (dashed) contours indicate positive (negative) SLP Laplacian. Bottom panel: Colormap of 10 m wind convergence (s^{-1}) overlaid with contours of SLP Laplacian that are the same as top panel.

4.3. SST-latent heat flux coupling

The latent heat flux out of the ocean and into the atmosphere is a major source of energy for wintertime synoptic variability in the atmosphere (Konda et al., 2010). As such, the extent to which the distribution of SST, rather than intrinsic atmospheric variability, alters the amount of heat exchange is important. SST can affect the surface latent heat flux by changing the saturation humidity, by altering the stability of the ABL, and by the indirectly changing the wind speed variations via VMM. A warm sea surface increases the saturation water vapor mixing ratio (q_s), hence enhances the humidity difference between air and sea surface ($q_s - q_a$), leading to the evaporative cooling. Increased winds over warmer waters would also enhance evaporative cooling, thereby decreasing SST (negative feedback). We study this impact of SST distribution on turbulent heat flux by examining the linear relationship between spatial derivatives of latent heat flux (dLH = dLH/dx and dLH/dy) and SST (dSST = dSST/dx and dSST/dy) over the same active eddy region as with the SST-wind stress analysis. We examine the derivative fields because, on the oceanic mesoscale, SST and latent heat flux have an in-phase relationship (Nonaka and Xie, 2003; Tokinaga et al., 2009), and the spatial derivatives tend to focus on the effect of oceanic mesoscale (Seo et al., 2007).

In the KE region, a significant negative linear relationship between dLH and dSST is seen in Control SCOAR, Smoothed SCOAR, as well as in observation (Fig. 9a), with associated coupling coefficients of $s_l = -16.2 \pm 0.3$, $s_l = -17.5 \pm 0.9$, $s_l = -13.1 \pm 0.6$ respectively for a typical winter month, January 2006. This reinforces the ability of SCOAR to simulate surface flux coupling in this region. Control SCOAR and Smoothed SCOAR have similar coupling coefficients, implying contributions of both
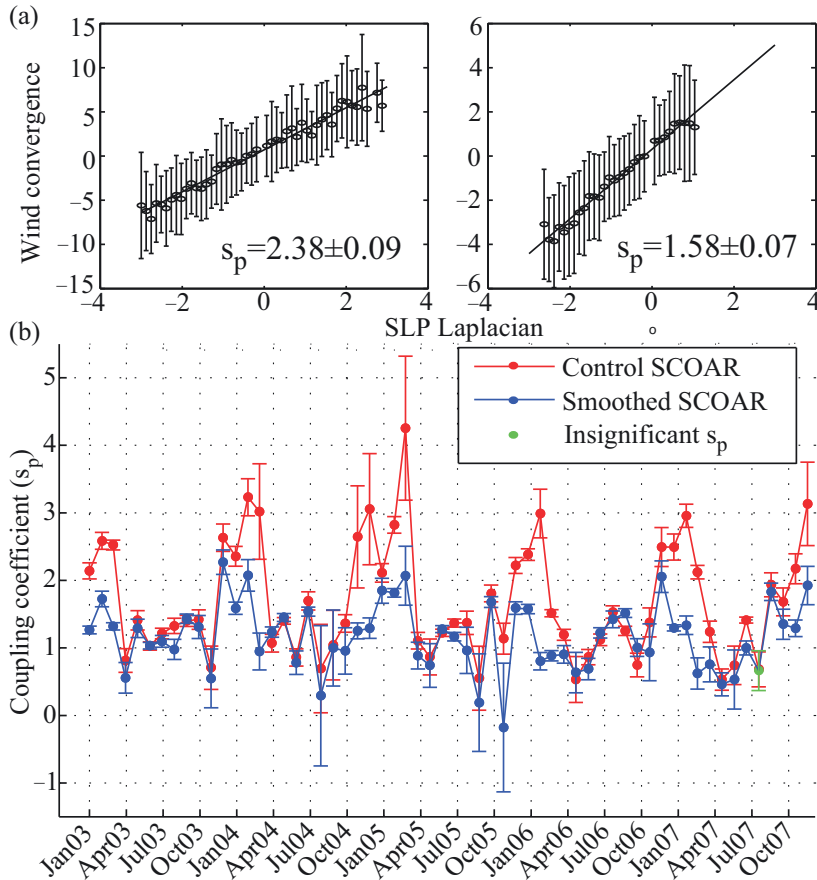
Fig. 8. (a) Linear fits to bin-scatter plot of 10 m wind convergence (10^{-6} s^{-1} against SLP Laplacian (10^{-9} Pa m^{-2}), over the same time period and domain of Fig. 2a, for Control SCOAR ((left) and Smoothed SCOAR (right), with coupling coefficients (s_p). (b) Time series of monthly s_p for 2003–2007 for Control SCOAR (red) and Smoothed SCOAR (blue). Error bars represent standard error of the slopes. Green dots indicate s_p with r^2 value smaller than 0.5 and p-value greater than 0.05. (For interpretation of the references to color in this figure legend, the reader is referred to the web version of the article.)

large-scale and mesoscale coupling to the surface heat flux–SST relationship. The coupling between surface heat fluxes and SST is significant year-round (Fig. 9b). There is also a clear seasonal cycle to the coupling, with the steepest negative relation in winter and weak coupling in summer, due to the seasonal differences in vertical stability of the atmosphere and possibly due to the deeper ABL in winter months. A similar seasonal cycle is also found with the use of anomalous latent heat flux (LH′) and SST′ (not shown), which have peak intensity during the winter months. Based on LH′ and SST′, we find averaged winter (DJF) coupling coefficients of $s_l = -14 \pm 3$ and $s_l = -13 \pm 4$ for Control and Smoothed SCOAR, respectively. This is similar to the corresponding winter-averaged coupling coefficients derived from the derivative fields, which are $s_l = -17 \pm 4$ and $s_l = -16 \pm 4$. This indicates that both large-scale and mesoscale coupling are important to the relationship between SST and latent heat flux. From Fig. 9b, it is also noted that the amplitude of the variability of s_l in the observations is smaller than in the model, with weaker coupling (factor of 0.7) in winter months and stronger coupling in summer months (factor of 2.0) for the observations, compared to model output. Similar results are obtained for sensible heat flux and SST gradient coupling (not shown).
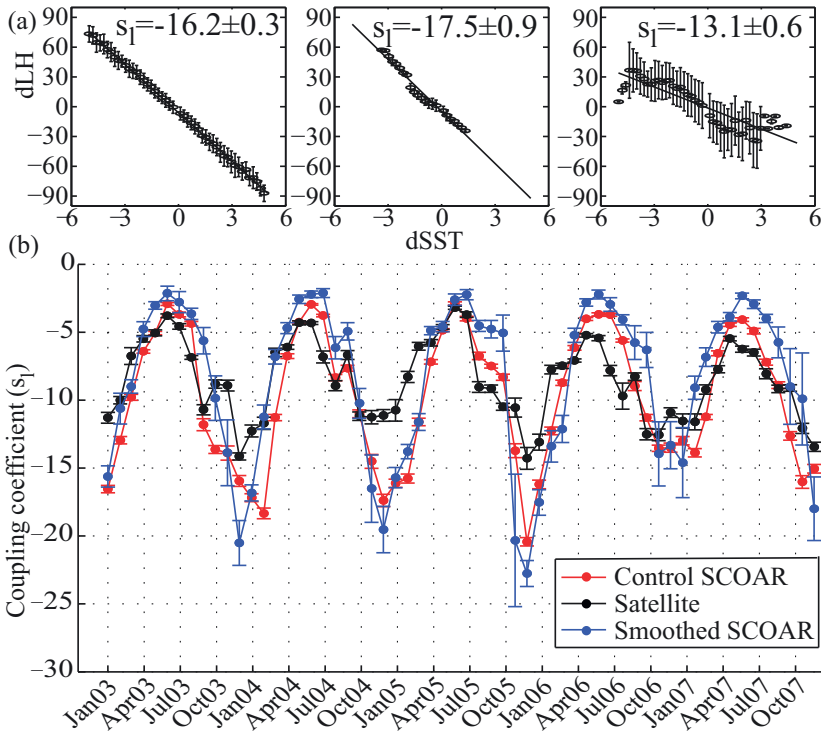
Fig. 9. (a) Linear fits of the bin-scatter plots of spatial derivatives of latent heat flux (W/m^2 per 100 km) and SST spatial derivatives (°C per 100 km) over the same time period and domain of Fig. 2a, for Control SCOAR (left), Smoothed SCOAR (middle) and observations (right), with coupling coefficients (s_l). (b) Time series of monthly s_l for 2003–2007, for Control SCOAR (red), Smoothed SCOAR (blue) and observations (black). Solid dots indicate values that have r^2 value greater than 0.5 and p-value less than 0.05. (For interpretation of the references to color in this figure legend, the reader is referred to the web version of the article.)

4.4. Mesoscale precipitation

Since mesoscale ocean–atmosphere interactions play a significant role in the KE region, a deterministic approach is adopted by performing a comparative study between the Control SCOAR run and the Smoothed RSM run to investigate the role of mesoscale SST on atmospheric processes, such as precipitation. We focus on one month during winter when the signal is particularly strong, based on an inspection of all the winter months that exhibited mesoscale precipitation anomalies. Fig. 10 gives a picture of the SST difference between the two runs, as well as the percentage of precipitation (PPT) difference for January 2001. The SST difference ranges between ±5 °C within an intensified region (KEPPT region; 144–156° E, 37–42° N; boxed domain in lower panel of Fig. 10) that corresponds to ±40% change in precipitation compared to the Control SCOAR. A transect at 40.5° N (black line in top panel of Fig. 10) is chosen to study the vertical structure of the atmosphere and its relation to SST and precipitation.

Precipitation is often associated with convection of moist air that reaches saturation and rains out. Over open water, warmer SST sets up a low pressure anomaly and low level wind convergence, which in turn induces convection and brings moist surface air to heights where it will cool and reach saturation, and then rain out. Through such a mechanism, an alignment of SST, low-level wind convergence and precipitation would be expected.

Fig. 11 (top) shows the vertical cross section of difference in wind divergence between Control SCOAR and Smoothed RSM, overlaid with difference in precipitation (black) and difference in SST
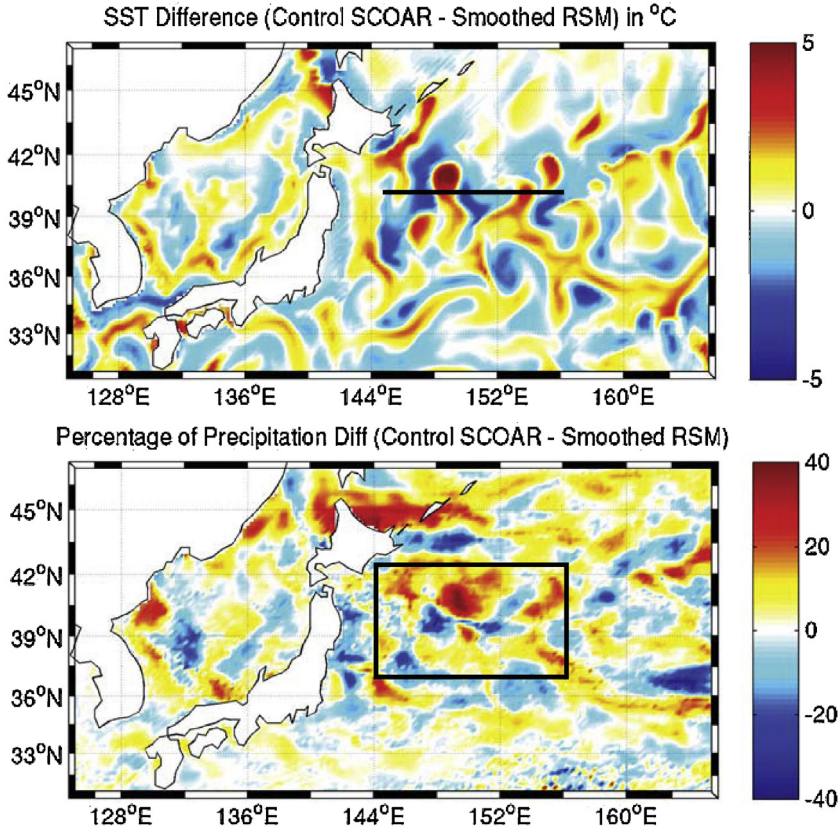
Fig. 10. Difference in SST [°C] distribution (top) of Control SCOAR – Smoothed RSM for January 2001. Corresponding distribution of percentage difference in precipitation [mm/day] (bottom). Location of 40.5° transect and intensified mesoscale region [boxed domain; 144–156° E, 37–42° N] marked on top and bottom figures respectively.

(red), averaged over January 2001. Mesoscale precipitation peaks at 146.5° E, 149.5° E and 154° E align well with low-level wind convergence (negative divergence) zone, but not SST maxima. Instead, peak precipitation coincides with negative gradients in SST. This can be attributed to the vertical mixing mechanism, rather than PAM, that induces low-level wind convergence along negative SST gradients (Fig. 2a), which in turn enhances the upward motion that allows for cloud formation and precipitation. This is further illustrated by the bottom figure of Fig. 11 that shows the cross section of the difference in vertical pressure velocity (Pa/s) for the same transect. Upward motion (negative vertical pressure velocity) coincides with precipitation maxima and along negative SST gradients, so as to suggest that convection is induced by low-level wind convergence that arose on the downwind side of positive SST anomalies.

The top panel of Fig. 12 shows the distribution of precipitation difference between Control SCOAR and Smoothed RSM, overlaid with contours of SST difference, in the KEPPT region. Peaks and troughs of precipitation difference are not well collocated with the mesoscale SST features. Instead, precipitation peaks and troughs have some alignment with maxima and minima in 10 m wind convergence difference, as seen in the middle panel of Fig. 12. This suggests that surface wind convergence, driven by the oceanic mesoscale SST, has an impact on precipitation. The lower panel on Fig. 12 is the difference in mesoscale 10 m wind convergence overlaid with downwind SST gradient difference. Positive (negative) wind convergence generally collocates
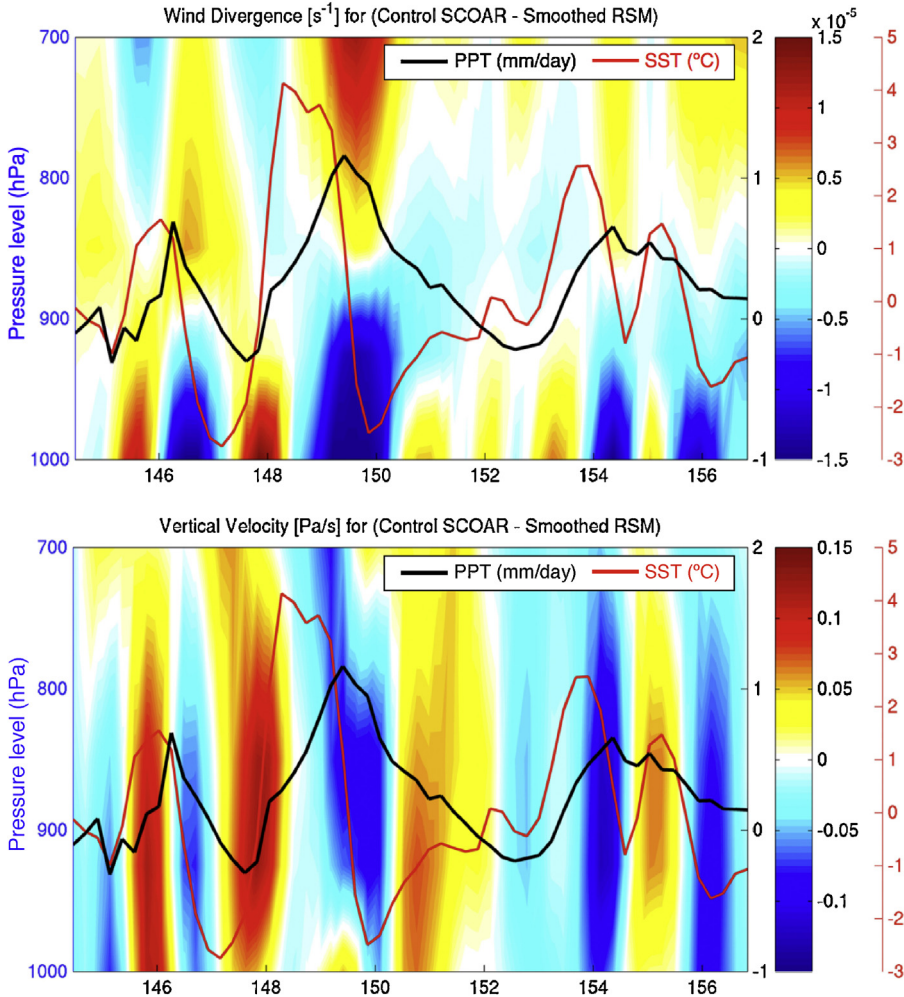
Fig. 11. Top: Vertical cross section of the difference in wind divergence [s⁻¹] from Control SCOAR – Smoothed RSM, at (144–156°
E, 40.5° N) for January 2001. There is an overlay with SST difference (°C; red) and precipitation difference (mm/day; black)
from Control SCOAR. Bottom: Same as top except colors reflect difference in vertical velocity (Pa/s). (For interpretation of the
references to color in this figure legend, the reader is referred to the web version of the article.)

along downwind gradient of negative (positive) SST, suggesting that the mesoscale surface wind
convergence is driven by the gradients in mesoscale SST through vertical mixing.

Based on Fig. 12, scatterplots of precipitation difference against SST difference, and precipita-
tion difference against 10 m wind convergence difference are made (Fig. 13). A linear regression
is performed on each scatterplot and their respective coupling coefficients (slope to the linear fit)
are computed, along with their corresponding r^2 coefficients. The coupling coefficient for precip-
itation difference against SST difference is found to be 0.06 mm/day per °C, but the large spread
of data points resulted in an associated r^2 of only 0.13, indicating that the coupling is insignifi-
cant. As for precipitation difference against mesoscale 10 m wind convergence difference, the data
spreads less and the coupling coefficient is found to be 0.21 mm/day per °C, with $r^2 = 0.44$. This
demonstrates that 44% of the variance in precipitation is explained by surface wind convergence
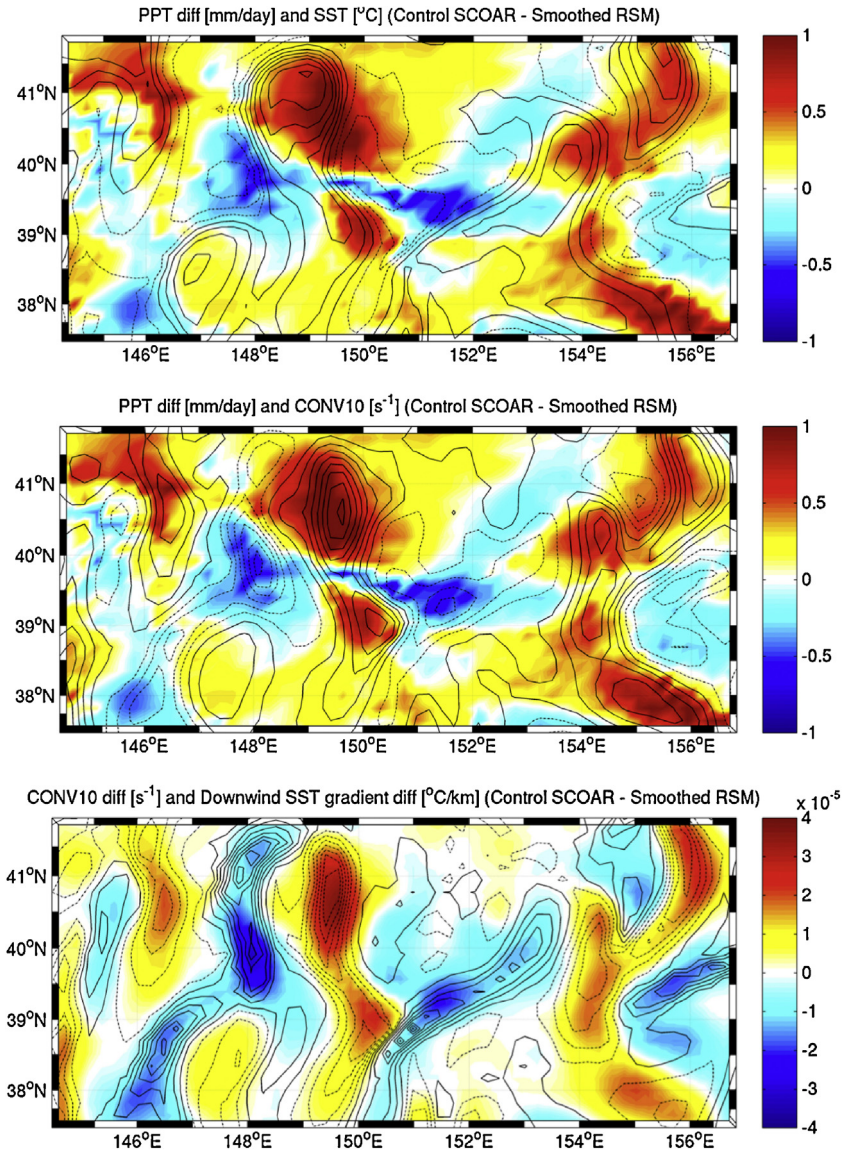driven by the gradients in mesoscale SST, a remarkable result given the nonlinearity of atmospheric

Fig. 12. Colormap of precipitation (PPT) difference [mm/day] of Control SCOAR – Smoothed RSM for January 2001, overlaid with contours of 1 °C SST difference (top panel). Solid (dashed) contours indicate positive (negative) SST difference. Middle panel has the same colormap of PPT difference, but overlaid with contours of difference in 10 m wind convergence [s^{-1}]. Similarly, solid (dashed) contours represent positive (negative) wind convergence, with intervals of 5×10^{-6} s^{-1}. The bottom panel is a colormap of difference in 10 m wind convergence [s^{-1}] overlaid with contours of 1 °C/km downwind SST gradient difference. Solid (dashed) contours indicate positive (negative) downwind SST gradient difference.

processes that contribute to precipitation. We also computed the overall precipitation difference in the KEPPT region between Control SCOAR and Smoothed RSM to get an estimate of the importance of SST anomaly rectification of precipitation. The total precipitation increased by only 6% in the presence of ocean eddies, indicating only minor potential impacts on larger-scale atmospheric states.
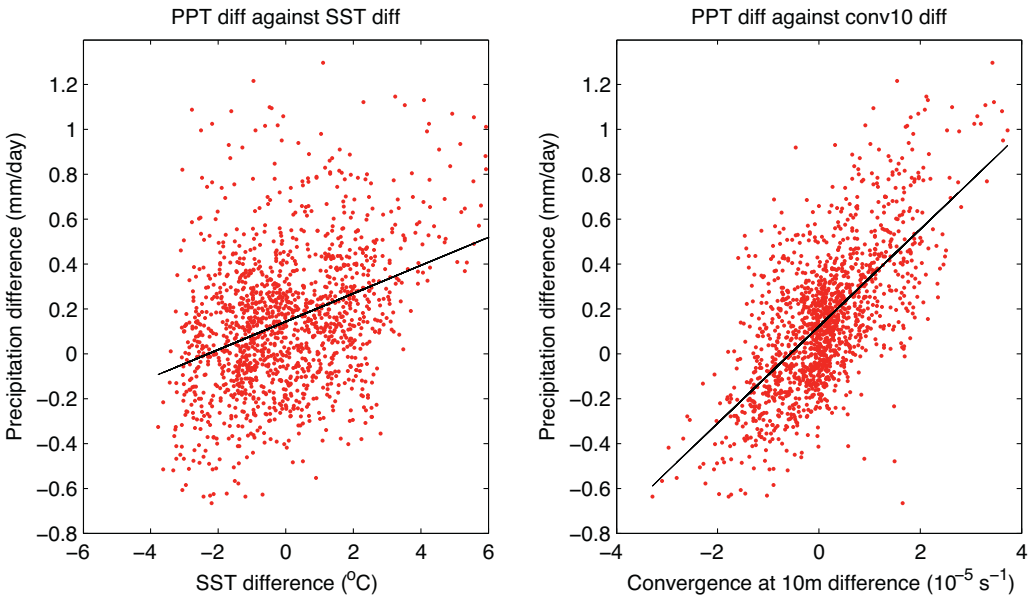
Fig. 13. Scatterplots of precipitation difference against SST difference (right panel) and precipitation difference against 10 m wind convergence difference (left panel), with linear regressions performed on each plot.

5. Summary

Regional coupled OA interactions were explored in the KE region using both observations and a coupled model. Within the KE region, the simulations reveal strong coupling between SST anomalies and winds, wind stresses and surface heat fluxes, with amplitudes, seasonal variations and wintertime maxima that exhibit many similarities with observations. Exploration of the importance of spatial scales on the strength and nature of the coupling was achieved by using a novel modeling strategy. A 2-D interactive spatial smoother, acting only on the SST seen by the atmosphere but not altering the actual oceanic state in any direct way, allows a straightforward analysis of the scale of OA coupling by comparing the output with a fully coupled run.

Two mechanisms of coupling were explored, the VMM and PAM. The Control SCOAR simulations reveal that both mechanisms are active and significant, especially in winter when the vertical stability of the atmosphere is weak. Differences in the strength of coupling between the Control and Smoothed SCOAR runs indicate how the spatial scale of SST fronts affects the OA coupling via these two mechanisms. Intuitively, one might expect that the VMM would be most active on the ocean mesoscale and less significant on the large scale. Instead, the models revealed that the VMM, as expressed in the coupling between downwind SST gradients and wind stress divergence, acts strongly on both the large scale and mesoscale. In this case, large-scale SST cannot be ignored. In contrast, the VMM, as expressed in the coupling between crosswind SST gradients and wind stress curl, is extinguished over large-scale SST gradients in Smoothed SCOAR. In this case, the ocean eddies are vital. For PAM, one might expect the large-scale coupling to be dominant. Instead, the PAM is far more active on the ocean mesoscale. For latent heat flux-SST coupling, both mesoscale and large-scale features are found to be important. More detailed study is in progress to explain the dynamics of these features.

The impact of mesoscale SST on precipitation was investigated for the month of January, 2001. Mesoscale SST anomalies do not collocate with precipitation anomalies, nor is there any direct coupling between SST and precipitation at the mesoscale. Rather, mesoscale downwind SST gradients are imprinted on the 10 m wind convergence anomalies, which are collocated with vertical velocity and precipitation anomalies. This suggests that mesoscale SST gradients induces surface wind

convergence anomalies through the vertical mixing mechanism, which in turn provide changes in vertical velocities that affect precipitation anomalies. However, we did not find any large-scale rectification effect of the oceanic mesoscale eddies on precipitation.

The role of mesoscale coupling on the evolution of oceanic instabilities and large-scale circulations has previously been explored using perturbation wind stress and wind stress curls (e.g. Spall, 2007; Hogg et al., 2009). The new technique introduced here opens the door for further studies to isolate the impact of ocean mesoscale eddies on the surface flux coupling processes with the atmosphere in other regions around the globe. It can also be extended to study the impact of the oceanic mesoscale on tropospheric response (e.g. Liu et al., 2007; Minobe et al., 2010), examine any rectified effect of precipitation or moisture fluxes by the mesoscale eddies and oceanic fronts (e.g. Xu et al., 2010), and consequent downstream ocean–atmosphere interactions (e.g. Taguchi et al., 2009; Frankignoul et al., 2011; Nakamura et al., 2004). Simulations are currently in progress to address these issues and their importance in decadal climate variability in the Pacific. Finally, the interactive smoothing technique can also be applied to the atmospheric forcing fields seen by the ocean to determine the feedback of the SST-induced flux anomalies on the ocean eddies themselves.

Acknowledgements

References

Bryan, F., Tomas, R., Dennis, J., Chelton, D., Loeb, N., McClean, J., 2010. Frontal scale air–sea interaction in high-resolution coupled climate models. J. Clim. 23, 6277–6291.

Cayan, D.R., 1992. Latent and sensible heat-flux anomalies over the Northern Oceans – driving the sea surface temperature. J. Phys. Oceanogr. 22, 859–881.

Chelton, D., Wentz, F., 2005. Global microwave satellite observations of sea surface temperature for numerical weather prediction and climate research. Bull. Am. Meteorol. Soc. 86, 1097–1115.

Chelton, D., Esbensen, S., Schlax, M., Thum, N., Freilich, M., Wentz, F., Gentemann, C.L., McPhaden, M., Schopf, P., 2001. Observations of coupling between surface wind stress and sea surface temperature in the eastern tropical Pacific. J. Clim. 14, 1479–1498.

Chelton, D., Schlax, M., Freilich, M., 2004. Satellite measurements reveal persistent small-scale features in ocean winds. Science 303, 978–983.

Chelton, D.B., Xie, S.-P., 2010. Coupled ocean-atmosphere interaction at oceanic mesoscales. Oceanography 23 (4), 52–69, http://dx.doi.org/10.5670/oceanog.2010.05.

Cleveland, W., 1979. Robust locally weighted regression and smoothing scatterplots. J. Am. Stat. Assoc. 74, 829–836.

De Szoeke, S.P., Bretherton, C.S., 2004. Quasi-Lagrangian large eddy simulations of cross-equatorial flow in the east pacific atmospheric boundary layer. J. Atmos. Sci. 61, 1837–1858.

Frankignoul, C., Sennechael, N., Kwon, Y.-O., Alexander, M., 2011. Influence of the meridional shifts of the Kuroshio and the Oyashio extensions on the atmospheric circulation. J. Clim. 24, 762–777.

Freilich, M., Long, D., Spencer, M., 1994. Seawinds: a scanning scatterometer for Adeos-II science overview. In: Proc. Int. Geoscience and Remote Sensing Symp., IEEE, pp. 960–963.

Haack, T., Chelton, D., Pullen, J., Doyle, J., Schlax, M., 2008. Summertime influence of SST on surface wind stress off the U.S. west coast from the U.S. Navy COAMPS model. J. Phys. Oceanogr. 38, 2414–2437.

Haidvogel, D.B., Arango, H., Budgell, W.P., Cornuelle, B.D., Curchitser, E., Di Lorenzo, E., Fennel, K., Geyer, W.R., Hermann, A.J., Lanerolle, L., Levin, J., McWilliams, J.C., Miller, A.J., Moore, A.M., Powell, T.M., Shchepetkin, A.F., Sherwood, C.R., Signell, R.P., Warner, J.C., Wilkin, J., 2008. Regional ocean forecasting in terrain-following coordinates: model formulation and skill assessment. J. Comput. Phys. 227, 3595–3624.

Hogg, A., Dewar, W., Berloff, P., Kravtsov, S., Hutchinson, D., 2009. The effects of mesoscale ocean–atmosphere coupling on the large-scale ocean circulation. J. Clim. 22, 4066–4082.

Juang, H.-M.H., Kanamitsu, M., 1994. The NMC nested regional spectral model. Mon. Weather Rev. 122, 3–26.

Kanamitsu, M., Ebisuzaki, W., Woolen, J., Potter, J., Fiorino, M., 2002. NCEP-DOE AMIP-II reanalysis (R-2). Bull. Am. Meteorol. Soc. 83, 1631–1643.

Konda, M., Ichikawa, H., Tomita, H., Cronin, M.F., 2010. Surface heat flux variations across the Kuroshio Extension as observed by surface flux buoys. J. Clim. 23, 5206–5221.

Kwon, Y.-O., Alexander, M., Bond, N., Frankignoul, C., Nakamura, H., Qiu, B., Thompson, L.A., 2010. Role of the gulf stream and Kuroshio–Oyashio systems in large-scale atmosphere ocean interaction: a review. J. Clim. 23, 3249–3281.

Latif, M., 2006. On North Pacific multidecadal climate variability. J. Clim. 19, 2906–2915.

Lindzen, R., Nigam, S., 1987. On the role of sea surface temperature gradients in forcing low-level winds and convergence in the tropics. J. Atmos. Sci. 44, 2418–2436.

Liu, W., Xie, X., Niiler, P., 2007. Ocean–atmosphere interaction over Agulhas extension meanders. J. Clim. 20, 5784–5797.

Miller, A., Schneider, N., 2000. Interdecadal climate regime dynamics in the North Pacific ocean: theories, observations and ecosystem impacts. Progr. Oceanogr. 47, 355–379.

Minobe, S., Kuwano-Yoshida, A., Komori, N., Xie, S.-P., Small, R., 2008. Influence of the Gulf Stream on the troposphere. Nature 452, 206–209.

Minobe, S., Miyashita, M., Kuwano-Yoshida, A., Tokinaga, H., Xie, S.-P., 2010. Atmospheric response to the Gulf Stream: seasonal variations. J. Clim. 23, 3699–3719.

Nakamura, H., Sampe, T., Tanimoto, Y., Shimpo, A., 2004. Observed associations among storm tracks, jet streams and midlatitude oceanic fronts, in Earth's Climate: The Ocean-Atmosphere Interaction, Geophysical Monograph, vol. 147, pp. 329–346, Ameri. Geophys. Union.

Nonaka, M., Xie, S.-P., 2003. Covariations of sea surface temperature and wind over the Kuroshio and its extension: evidence for ocean-to-atmosphere feedback. J. Clim. 16, 1404–1413.

O'Neill, L.W., Chelton, D.B., Esbensen, S.K., 2003. Observations of SST-induced perturbations of the wins stress field over the Southern Ocean on seasonal timescales. J. Clim. 16, 2340–2354.

Sasaki, H., Sasai, Y., Nonaka, M., Masumoto, Y., Kawahara, S., 2006. An eddy-resolving simulation of the quasi-global ocean driven by satellite-observed wind field: preliminary outcomes from physical and biological fields. J. Earth Simul. 6, 34–49.

Schlax, M., Chelton, D., Freilich, M., 2001. Sampling errors in wind fields constructed from single and tandem scatterometer datasets. J. Atmos. Ocean. Technol. 18, 1014–1036.

Seo, H., Miller, A., Roads, J., 2007. The Scripps Coupled Ocean–Atmosphere Regional (SCOAR) model, with applications in the eastern pacific sector. J. Clim. 20, 381–402.

Seo, H., Murtugudde, R., Jochum, M., Miller, A., 2008. Modeling of mesoscale coupled ocean–atmosphere interaction and its feedback to ocean in the western Arabian sea. Ocean Model. 25, 120–131.

Seo, H., Jochum, M., Murtugudde, R., Miller, A.J., 2006. Effect of ocean mesoscale variability on the mean state of tropical Atlantic climate. Geophys. Res. Lett., 33.

Shchepetkin, A., McWilliams, J., 2005. The regional oceanic modeling system (ROMS): a split-explicit, free-surface, topography-following-coordinate ocean model. Ocean Model. 9, 347–404.

Shimada, T., Minobe, S., 2011. Global analysis of the pressure adjustment mechanism over sea surface temperature fronts using airs/aqua data. Geophys. Res. Lett. 38.

Small, R., de Szoeke, S., O'Neill, L., Seo, H., Song, Q., Cornillon, P., Spall, M., Minobe, S., 2008. Air–sea interaction over ocean fronts and eddies. Dyn. Atmos. Oceans 45, 274–319.

Spall, M., 2007. Notes and correspondence: effect of sea surface temperature wind stress coupling on baroclinic instability in the ocean. J. Phys. Oceanogr. 37, 1092–1097.

Taguchi, B., Nakamura, H., Nonaka, M., Xie, S.-P., 2009. Influences of the Kuroshio/Oyashio extensions on air–sea heat exchanges and storm-track activity as revealed in regional atmospheric model simulations for the 2003/04 cold season. J. Clim. 22, 6536–6560.

Taguchi, B., Nakamura, H., Nonaka, M., Komori, N., Kuwano-Yoshida, A., Takaya, K., Goto, A., 2012. Seasonal evolutions of atmospheric response to decadal SST anomalies in the North Pacific Subarctic Frontal zone: observations and a coupled model simulation. J. Clim. 25, 111–139.

Takatama, K., Minobe, S., Inatsu, M., Xie, S.-P., Small, R., 2011. Diagnostics for near-surface wind convergence/divergence response to the Gulf Stream in a regional atmospheric model. Atmos. Sci. Lett. 12, 206–209.

Thum, N., Esbensen, S., Chelton, D., McPhaden, M., 2002. Airsea heat exchange along the northern sea surface temperature front in the eastern tropical pacific. J. Clim. 15, 3361–3378.

Tokinaga, H., Tanimoto, Y., Xie, S.-P., Sampe, T., Tomita, H., Ichikawa, H., 2009. Ocean frontal effects on the vertical development of clouds over the western North Pacific: in situ and satellite observations. J. Clim. 22, 4241–4260.

Vecchi, G., Xie, S., Fischer, A., 2004. Ocean–atmosphere covariability in the western Arabian sea. J. Clim. 17, 1213–1224.

Wallace, J., Mitchell, T., Deser, C., 1989. The influence of sea surface temperature on surface wind in the eastern equatorial pacific: seasonal and interannual variability. J. Clim. 2, 1492–1499.

Wentz, F., Gentemann, C., Smith, D., Chelton, D., 2000. Satellite measurements of sea surface temperature through clouds. Science 288, 847–850.

Wu, R.G., Kirtman, B.P., Pegion, K., 2006. Local air–sea relationship in observations and model simulations. J. Clim. 19, 4914–4932.

Xie, S.-P., 2004. Satellite observations of cool ocean–atmosphere interaction. Bull. Am. Meteor. Soc. 85, 195–209.

Xu, H., Tokinaga, H., Xie, S.-P., 2010. Atmospheric effects of the Kuroshio large meander during 2004-05. J. Clim 23, 4704–4715.

Yu, C., Weller, R., 2007. Objectively analyzed air–sea heat fluxes for the global OCE-free oceans (1981–2005). Bull. Am. Meteorol. Soc. 88, 527–539.